

# A Recipe for Electrically-Driven Soft Robots via 3D Printed Handed Shearing Auxetics

Ryan L. Truby , Lillian Chin , and Daniela Rus 

**Abstract**—Electrically-mediated actuation schemes offer great promise beyond popular pneumatic and suction based ones in soft robotics. However, they often rely on bespoke materials and manufacturing approaches that constrain design flexibility and widespread adoption. Following the recent introduction of a class of architected materials called handed shearing auxetics (HSAs), we present a 3D printing method for rapidly fabricating HSAs and HSA-based soft robots that can be directly driven by servo motors. To date, HSA fabrication has been limited to the laser cutting of extruded teflon tubes. Our work expands the HSA materials palette to include flexible and elastomeric polyurethanes. Herein, we investigate the influence of material composition and geometry on printed HSAs' mechanical behavior. In addition to individual HSA performance, we evaluate printed HSAs in two soft robotic systems - four degree-of-freedom (DoF) platforms and soft grippers - to confirm that printed HSAs perform similarly to the original teflon HSA designs. Finally, we demonstrate new soft robotic capabilities with 3D printed HSAs, including fully 3D printed HSA fingers, higher force generation in multi-DoF devices, and demonstrations of soft grippers with internal HSA endoskeletons. We anticipate our methods will expedite the design and integration of novel HSAs in electrically-driven soft robots and facilitate broader adoption of HSAs in the field.

**Index Terms**—Soft robot materials and design, soft sensors and actuators, additive manufacturing.

## I. INTRODUCTION

ONE of the current pressing challenges of soft robotics is identifying methods for actuating soft materials in a way that complements the compliance of soft robots' bodies. Despite the popularity of pneumatic- and vacuum-based actuation techniques, these strategies typically rely on pumps and other bulky, rigid hardware components to achieve complex motions. These auxiliary components consistently complicate the systems-level design of integrated soft robots, limiting their deployment in

practice [1], [2]. New electrically-mediated actuation schemes with minimal hardware requirements are needed in soft robotics.

In order to minimize burdensome auxiliary hardware, current research has sought to streamline soft robotic actuation through the design of new material functionalities that better enable electrically-driven actuation. Electrostatic actuation [3], [4] and the Joule heating of thermally responsive materials [5]–[7] are two such approaches, but still suffer from many design and operational limitations. For example, dielectric elastomer actuators and other soft electrostatic transducers enable rapid, energy efficient actuation, but they are tedious to fabricate and require large voltages that pose safety risks and design challenges [3], [4]. Meanwhile, Joule heating materials like liquid crystal elastomer actuators can lead to large actuation strains and high forces, but thermally actuated systems are slow and non-trivial to reverse [6], [7].

Recent progress in mechanical metamaterial design suggests another promising approach towards simplifying and/or improving soft robotic actuation. Architected material forms can give rise not only to compliance and other programmable mechanical properties, but also to structures with emergent robotic behaviors [8]. For example, structures with reversible buckling, bistability, or auxetic properties [9] could be used in soft robot design for rapid motion in compliant structures [10], [11], programmable deformations and shape change [12], tunable stiffness, and even mechanical logic and sensing [13], [14]. Although advances in structural metamaterial designs offer great promise for soft robotics, these ideas have not yet been fully or extensively applied for improving actuation. Many of the actuation strategies currently demonstrated in architected materials fall into the same issues as more traditional soft robotic actuation schemes; they either only provide a one-shot actuation [15], [16] or require bulky hardware that significantly limits soft robots' practical use [11], [12], [17]–[19]. Moreover, while progress in digital and additive manufacturing [20] and computational design and optimization tools [21], [22] have fueled much of the recent progress in this field, most demonstrations of architected mechanical metamaterials for soft robotics require bespoke materials and manufacturing methods that not only constrain design flexibility, but also limit adoption by others in the research community. There is a clear need and opportunity for a new strategy towards soft robotic actuation via architected metamaterials, especially one that maximizes material design flexibility, minimizes auxiliary hardware, and uses more accessible fabrication methods.

To address this need, we present methods and materials for 3D printing custom handed shearing auxetics (HSAs), a chiral cellular metamaterial structure that can be directly actuated

Manuscript received October 22, 2020; accepted December 21, 2020. Date of publication January 18, 2021; date of current version February 1, 2021. This letter was recommended for publication by Associate Editor R. MacCurdy and Editor K.-J. Cho upon evaluation of the reviewers' comments. The work of Ryan L. Truby was supported by the Schmidt Science Fellows program, in partnership with the Rhodes Trust. The work of Lillian Chin was supported by the National Science Foundation Graduate Research Fellowship under Grant #1122374, and the Fannie, and John Hertz Foundation. This work was supported through the NSF EFRI Program under Grant #1830901. (Ryan L. Truby and Lillian Chin contributed equally to this work.) (Corresponding author: Ryan L. Truby.)

The authors are with the MIT Computer Science and Artificial Intelligence Laboratory, Massachusetts Institute of Technology, Cambridge, MA 02139 USA (e-mail: rltruby@mit.edu; litchin@mit.edu; rus@csail.mit.edu).

This article has supplementary downloadable material available at <https://doi.org/10.1109/LRA.2021.3052422>, provided by the authors.

Digital Object Identifier 10.1109/LRA.2021.3052422



Fig. 1. A recipe for electrically-driven soft robots via 3D printed HSAs. Step 1: HSAs are 3D printed via digital projection lithography. The photograph shows a complete HSA finger at the end of 3D printing. Step 2: Parts are post-processed. A final HSA finger is shown. Step 3: Parts are integrated into soft robots. 3D printed HSAs are used in (i) 4-DoF, soft robotic platforms and (ii) assembled into bending actuators as HSA fingers in soft grippers. Scale bars are 25 mm, except in Step 2, where the scale bar is 10 mm.

with servo motors (Fig. 1). These actuators have demonstrated significant promise as an actuation strategy for soft robotics, achieving similar performance to traditional soft robotic systems and manipulators with significantly improved energy efficiency and resiliency to mechanical damage [23]–[25]. However, like other architected materials, they have suffered from significant fabrication limitations. To date, suitable HSAs for soft robots have only been fabricated by laser cutting teflon, or polytetrafluoroethylene (PTFE), tubing. This fabrication method has restricted the exploration of HSA designs to planar and wrapped-planar systems with a material that is difficult to process accurately. An additive manufacturing approach would enable new complex 3D designs with greater material selection. We address these concerns by demonstrating successful fabrication of HSAs from various polyurethane formulations, creating a range of rigid, flexible, and elastomeric HSAs. We investigate the impact of key architectural and material parameters in printed HSAs on their mechanical behaviors and contrast them with original PTFE designs. We perform this comparison in both single HSAs and on 4-DoF platforms and soft grippers, which represent examples of soft robots comprised of HSA actuators. Finally, we demonstrate the new expanded design space of 3D printed HSAs by showcasing more custom applications, including fully 3D printed HSA assemblies for soft robotic manipulators, concentrically assembled HSAs for generating higher force without requiring torque increases from servo motors, and hybrid rigid-soft HSA actuators with stabilizing endoskeletons. Overall, our paper contributes the following:

TABLE I  
MECHANICAL PROPERTIES OF HSA MATERIALS

	PTFE [26]	RPU [27]	FPU [28]	EPU [29]
<b>Hardness, Shore A/D</b>	50-65D	80D	71D	68A
<b>Elastic Modulus</b>	392 MPa	1700 MPa	700 MPa	8 MPa
<b>Ultimate Tensile Strength</b>	21-35 MPa	40 MPa	25 MPa	9 MPa
<b>Elongation at Break</b>	300-500%	30%	200%	300%
<b>Flexural Modulus</b>	490-588 MPa	1500 MPa	800 MPa	N/A

- A 3D printing approach for rapidly fabricating custom shearing auxetics and integrated HSA assemblies for electrically-driven soft robots,
- An expanded materials palette for HSAs that includes flexible and elastomeric polyurethanes,
- An investigation of the impacts of various geometric parameters and materials on HSAs' mechanical properties, and
- Examples of HSA-based soft robots with new capabilities, including higher force generation and stabilizing endoskeletons.

## II. DESIGN AND EXPERIMENTAL METHODS

### A. Original HSA Design and Fabrication

HSAs are a class of auxetic metamaterials introduced in [25] and used for soft robotic actuation in [23]. While typical auxetic metamaterials have a symmetric point in their trajectory, allowing them to move from one handedness to another, HSAs intentionally break that symmetry to only allow a single chiral shear motion. Thus, left- and right-handed HSAs can be made through a simple reflection of the cellular pattern. When placed around a cylinder, this handed shear movement creates a strong coupling between rotation with extension. A soft linear actuator can then be created by pairing cylinders of opposite handedness so each one counters the other's rotation.

In order to achieve these effects, the HSA must be able to open smoothly from its closed state, making the form and mechanical properties of its living hinges critical to its auxetic behavior. As seen in Fig. 2(a), the metamaterial structure of an HSA is composed of many individual struts joined by these living hinges. The joints should act similarly to pin joints and, therefore, be thin, flexible, and able to accommodate high strains. Living hinges that cannot accommodate high strain or are too rigid will restrict bending or yield under a net torque acting on the HSA, resulting in limited actuation or failure of the actuator, respectively. These design constraints led to the initial material choice of PTFE for HSAs, which has a high elongation at break of 300-500% (Table I) [26]. This allowed the living hinges to plastically deform and buckle out-of-plane as the HSA elongated without fear of joint snapping. PTFE is also available off-the-shelf as tubes, enabling HSAs to be fabricated via rotary laser cutting to achieve satisfactorily thin features. However, reliance on off-the-shelf materials introduced significant variance in HSA behavior. The lack of precision engineering tolerances

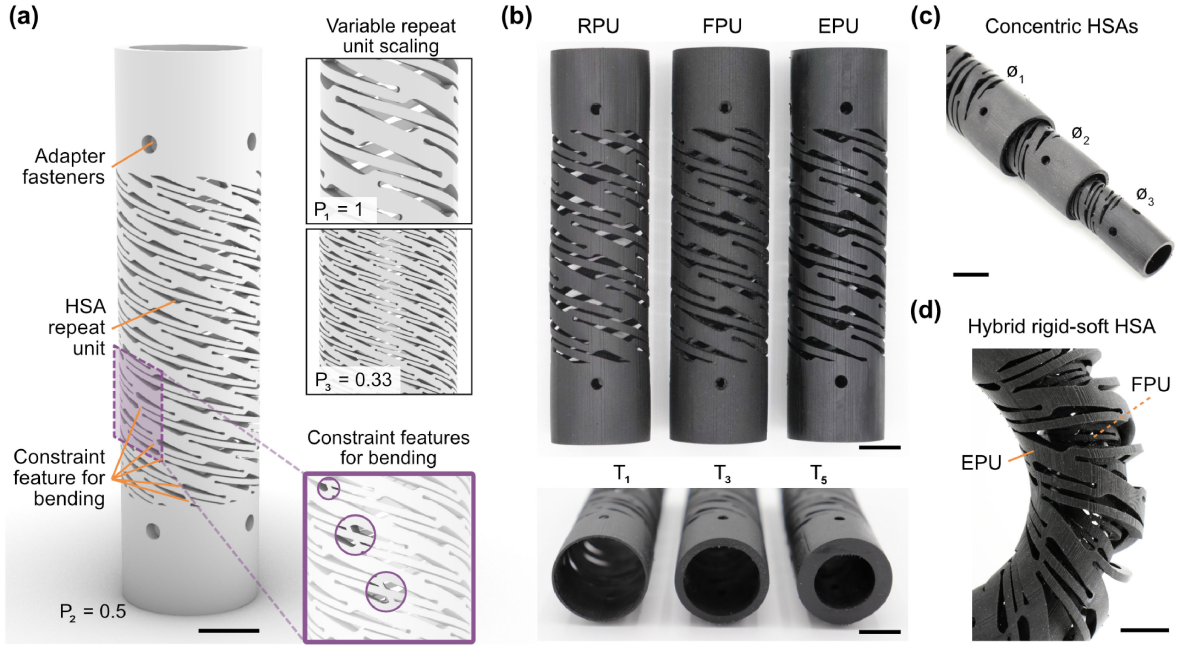


Fig. 2. HSA Design. (a) The leftmost illustration shows a representative HSA design explored in this work (with outer diameter,  $\phi$ , of 25.4 mm), indicating the form of the HSA repeat units in the structure, the location of the adapter fasteners to servo motors, and representative forms of constraint features added for directional bending in bending HSAs (shown in higher detail in the inset to the lower right). All HSAs explored are printed with the same length ( $L = 101.6$  mm), number and position of adapter fasteners, and area of HSA repeat unit patterns that are shown at left. HSAs with patterns of repeat units scaled to different sizes were explored. To the upper right, magnified views of HSAs with the original pattern scaling introduced in Ref. [23] ( $P_1 = 1$ ) and a scaling of  $1/3$  ( $P_3 = 0.33$ ) are indicated in the top and bottom images, respectively. The HSA illustration to the left has a repeat unit scaling of  $1/2$  ( $P_2 = 0.5$ ). (b) Photographs of RPU (left), FPU (center), and EPU (right) HSAs are provided for top-down (top) and end-on (bottom) views. In these photos, the RPU, FPU, and EPU HSAs are printed with a thickness of 0.79 mm ( $T_1$ ), 2.48 mm ( $T_3$ ), and 4.76 mm ( $T_5$ ), respectively. (c) HSAs of varying  $\phi$  can be concentrically arranged together. Three FPU HSAs printed with thickness of 1.59 mm ( $T_2$ ) and decreasing outer diameters of  $\phi_1 = 25.4$  mm,  $\phi_2 = 20.3$  mm, and  $\phi_3 = 15.2$  mm are shown. (d) A close-up view of a hybrid rigid-soft bending HSA is shown. The rigid HSA has an exterior EPU HSA ( $T_4$ ,  $P_1$ ) and an interior FPU HSA with lower  $\phi$  ( $T_3$ ,  $P_1$ ). Both have added constraint features for bending. Scale bars are 10 mm.

TABLE II  
ARCHITECTURAL FEATURES INVESTIGATED BY HSA MATERIAL

	PTFE	RPU	FPU	EPU
<b>HSA Outer Diameter,</b> $\phi$	$\phi_1 = 25.4$ mm	$\phi_1 = 25.4$ mm	$\phi_1 = 25.4$ mm $\phi_2 = 20.3$ mm $\phi_3 = 15.2$ mm	$\phi_1 = 25.4$ mm
<b>Cylindrical HSA Thickness,</b> $T$	$T_2 = 1.59$ mm	$T_1 = 0.79$ mm $T_2 = 1.59$ mm $T_3 = 2.48$ mm $T_4 = 3.18$ mm	$T_2 = 1.59$ mm $T_3 = 2.48$ mm $T_4 = 3.18$ mm	$T_4 = 3.18$ mm $T_5 = 4.76$ mm $T_6 = 6.35$ mm
<b>Repeat Unit Scaling,</b> $P$	$P_1 = 1$ (100%)	$P_1 = 1$ (100%)	$P_1 = 1$ (100%) $P_2 = 0.5$ (50%) $P_3 = 0.33$ (33%)	$P_1 = 1$ (100%)
<b>HSA Designs Fabricated</b>	w/out constraints w/ constraints for bending	w/out constraints	w/out constraints w/ constraints for bending Concentric HSAs Hybrid HSA	w/out constraints w/ constraints for bending Hybrid HSA

for both the extruded PTFE tubes' dimensions and the rotary laser cutting hardware's accuracy meant that joints and strut sizes could not be precisely standardized.

In this paper, we use the PTFE cylinder from [23] as the starting point of our 3D printed designs. PTFE HSAs are cut from 25.4 mm diameter PTFE tubes with a 2.43 mm wall thickness (McMaster Carr) on a 120 W laser cutter with rotary engraver attachment (Universal Laser Systems). The base auxetic units are repeated three times around the circumference of each cylinder. Bending actuators are created by placing a constraint feature along the diagonal of the HSA pattern to limit expansion (Fig. 2(a)).

### B. 3D Printing HSAs

We investigate HSAs based on the form presented in [23] and shown in Fig. 2(a). HSAs are designed in Rhino 6 and Grasshopper (Robert McNeel & Associates). The architectural features we explore in our HSA designs – material, outer diameter ( $\phi$ ), thickness ( $T$ ), repeat unit scaling ( $P$ ), and length ( $L$ ) – are summarized in Table II. Briefly, the HSA repeat unit is patterned within the same area to form the living hinge network that enables auxetic behavior during actuation. The geometry of the repeat unit itself is unchanged and identical to that in previous HSAs [23], except for scaling in certain variants (100%, 50% or

33% of original size as  $P_1$ ,  $P_2$ , and  $P_3$ , respectively). All HSAs have  $L = 101.6$  mm.

HSAs are 3D printed via digital projection lithography (Carbon M1, Carbon Inc.) from three commercially available, proprietary photopolymer resins: RPU 70, FPU 50, and EPU 40, which are rigid (RPU), flexible (FPU), and elastomeric polyurethane (EPU) resins, respectively (Carbon Inc.). The resins are used as received. HSAs are printed horizontally with supports to reduce print time. After printing, HSAs are carefully handled and processed according to the manufacturer's instructions, ensuring minimal deformation. The mechanical properties of RPU, FPU, and EPU are provided in Table I.

Printed HSAs are first formed in a green body state through photopolymerization of resins during the printing process, after which they undergo a final thermal curing step. In the green body state, RPU, FPU, and EPU HSAs are mechanically quite different: RPU HSAs are more robust than FPU HSAs of the same thickness, and EPU HSAs, while being the most resilient to deformations, are prone to tearing during support removal if too thin. Thus, printing HSAs from each material was limited to the thicknesses listed in Table II.

### C. Mechanical Characterization

The HSAs' extensional and hysteretic behaviors are characterized by tensile and cyclic extension tests, respectively. For all tests, HSAs are mounted to the Instron via custom, 3D printed adapters (printed from UMA 90 resin, Carbon Inc.) that keep one end of the HSA fixed while allowing for free rotation of the other [23]. In tensile extension tests, HSAs are linearly extended at 1 mm/s until failure. In cyclic extension tests, HSAs are cyclically extended to 50 mm at a rate of 10 mm/s (except for RPU HSAs, which had to be cycled at a slower rate of 1 mm/s). The 50 mm extension corresponds to a stretch,  $\lambda$ , of  $\lambda \approx 0.5$ , or actuation strain of 50%, for our HSAs, while the 10 mm/s extension rate reflects a typical actuation rate during operation in a HSA-based soft robot.

### D. Electrically-Driven Soft Robots

Previous examples of electrically-driven soft robots based on PTFE HSAs include 4-DoF platforms and parallel grippers [23], [25]. In this work, we present several variations of these soft platforms (Fig. 1 i) and grippers (Fig. 1 ii) using FPU and EPU HSAs. Briefly, the 4-DoF platforms consist of four HSAs in a  $2 \times 2$  configuration, where alternating HSAs have different handedness, the proximal end of each HSA is attached to a servo motor, and the distal ends are fixed together by a 3D-printed end adapter piece (printed from UMA 90 resin, Carbon Inc.). The soft grippers are similar to the soft platforms with respect to their configuration and fixing of HSA ends to servos and rigid end pieces. However, HSAs in soft grippers are of opposite handedness arranged in a  $2 \times 1$  configuration, and both HSAs have constraint features added within the repeat unit pattern to drive directional bending of the fingers for grasping (Fig. 2(a)) [23].

Three soft HSA platforms were assembled. Two platforms are comprised of four FPU and four EPU HSAs (FPU and EPU platforms) with thicknesses of  $T_3$  and  $T_5$ , respectively, for comparison with original soft platforms constructed from PTFE HSAs (PTFE platform). To highlight the ability to construct

devices from HSAs of custom size, a third soft platform was also developed from four concentrically assembled sets of three FPU HSAs (concentric platform), with varying outer diameters, but thickness kept at  $T_2$ . All platforms are driven by HS-785HB servos controlled by a Pololu Micro Maestro 6-Channel USB Servo Controller.

Lastly, two soft grippers were developed. The first is comprised of FPU HSAs, with two FPU HSAs of opposite handedness comprising one finger (thickness of  $T_3$ , HSA repeat unit scaling of  $P_3$ ). The second is a hybrid soft-rigid gripper comprised of concentrically arranged HSA assemblies, where the outer HSA is printed from EPU and the inner from FPU to form a rigid endoskeleton. The EPU and FPU HSAs in the hybrid gripper have thicknesses of  $T_5$  and  $T_3$ , respectively, and both have a repeat unit scaling of  $P_1$ . All soft grippers are developed for integration on a multiplexed manipulation platform introduced previously with PTFE HSAs [30]. They are driven by HS-5585MH servos controlled by an Arduino.

### E. Soft Robot Characterization

Qualitatively, the soft platforms are evaluated by visually comparing the platforms' responses to the same control sequence across all of its degrees of freedom: vertical extension and rotation about all axes. The same position commands were sent to the servos for each of the actions in the control sequence, ensuring any perceived variation results from material differences. Quantitatively, the concentric platform with and without its two inner HSAs is characterized by blocked force tests. In these experiments, the blocked force is measured via a static Instron load cell, which the distal end of the platform presses against. The servos are rotated in  $15^\circ$  increments for 5 s from  $0^\circ$  to  $180^\circ$  to elongate the platform against the load cell. At  $180^\circ$  rotation, the servos are then rotated in the opposite direction following the same procedure back to  $0^\circ$ . The blocked force is determined from the mean measurement over the 5 s hold at each servo rotation angle after removing the actuation transition periods.

For the soft grippers, the grasping force is characterized by measuring the amount of force needed to remove a 3D printed sphere from the gripper. In these experiments, the sphere is pulled out of the soft gripper's grasp at a rate of 5 mm/s as the Instron load cell measures the amount of force as a function of extension. The sphere was selected as a representative target object that would be held by such a manipulator. The mean grip force is determined from the average load cell measurement between extensions of 5 and 15 mm, while the max grip force is determined as the maximum force within that interval. All experiments for both the platforms and grippers are repeated five times to determine standard deviation.

## III. EXPERIMENTAL RESULTS

### A. 3D Printed Handed Shearing Auxetics

Our 3D printing method provides a more streamlined fabrication method than laser cutting, allowing more complex designs to be fabricated with ease. The digital projection lithography approach is appropriate for rapidly fabricating the 3D forms of HSAs. Unlike previous HSAs, which could only be created from

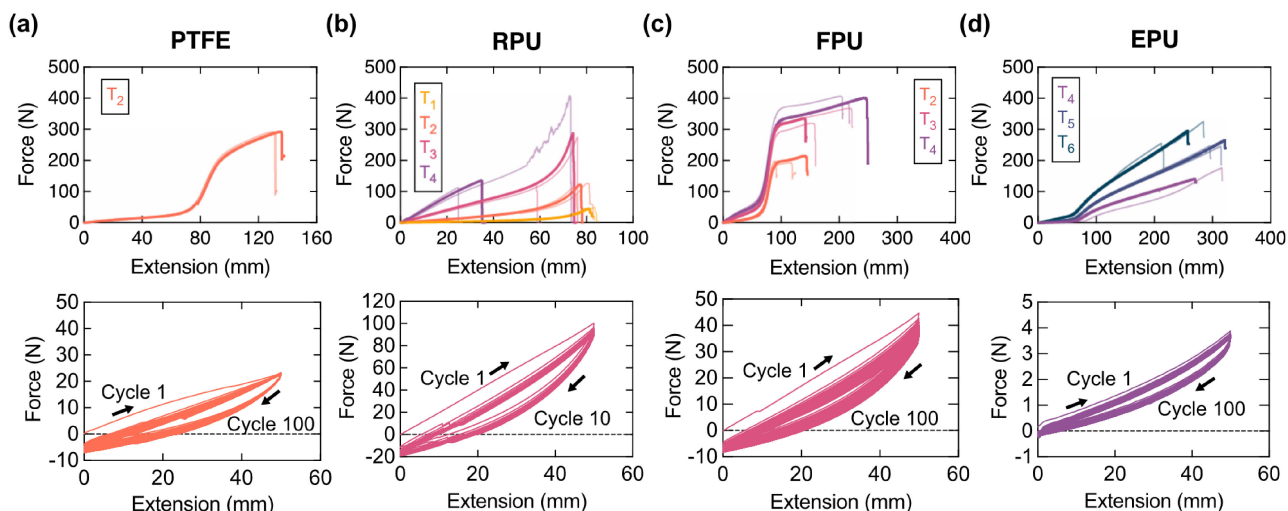


Fig. 3. HSA Mechanical Characterization. Data are organized by column for (a) PTFE, (b) RPU, (c) FPU, and (d) EPU HSAs. (Top row) Force versus extension data from tensile extension tests are provided for HSAs of varying thicknesses. Data are provided for three HSAs of each thickness. For improved visibility, one plot for a given thickness is provided as a thick line, while the other two are given as thinner, transparent ones. All axes are scaled identically, except for the  $x$  axes of PTFE and RPU data, to aid visualization. (Bottom row) Force versus extension data from cyclic extension tests are provided. Each plot corresponds to one HSA of a single thickness. PTFE, FPU, and EPU HSA cyclic tests are performed for 100 cycles at 10 mm/s extension rate; RPU HSA cyclic tests are for 10 cycles at 1 mm/s extension rate. All axes are scaled identically, except for the  $y$  axes of RPU and EPU data, to aid visualization.

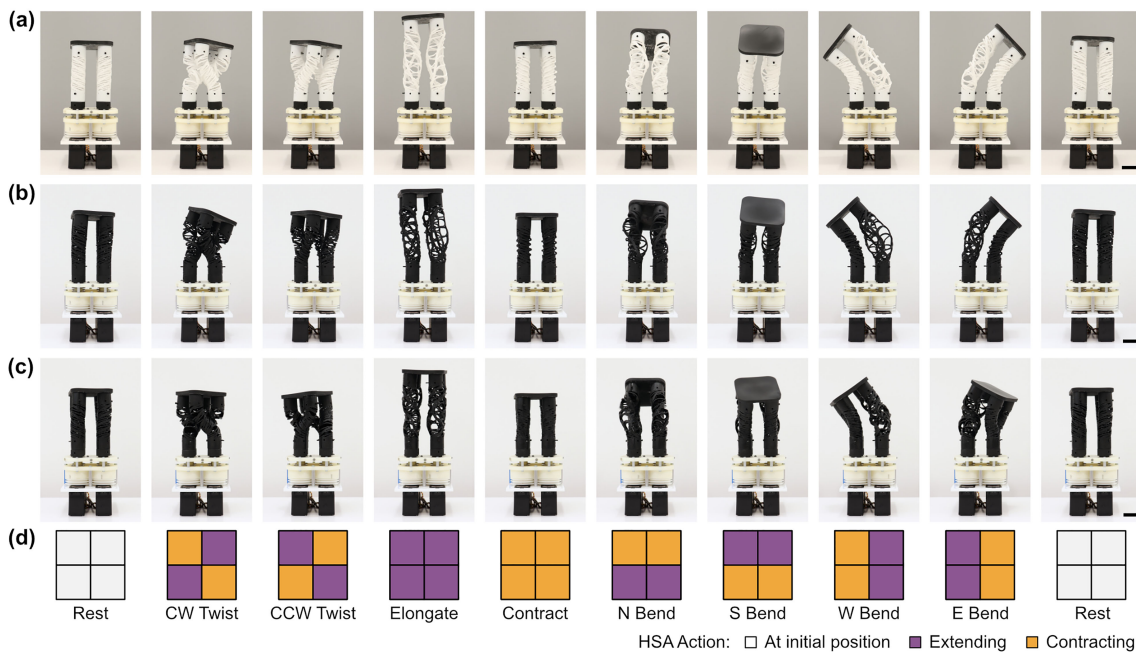


Fig. 4. Soft Robotic 4-DoF Platforms. (a–c) Photographs show soft platforms comprised of four HSAs composed of (a) PTFE, (b) FPU, or (c) EPU during different actions: clockwise (CW) twist, counter-clockwise (CCW) twist, elongate, contract, northward (N) bend, southward (S) bend, westward (W) bend, and eastward (E) bend. (d) Schematics of the HSA actions inducing the different configurations are shown. For each action, the same servo position command is sent across all materials. Scale bars are 25 mm.

stock PTFE cylinders, we are able to readily 3D print HSAs from RPU, FPU, and EPU resins (Fig. 2(b)). Furthermore, our 3D printing method makes custom HSA designs possible, ranging from concentric HSAs of varying  $\phi$  (Fig. 2(c)) and hybrid HSAs assembled by inserting a FPU HSA endoskeleton ( $\phi_3$ ) within an EPU HSA ( $\phi_1$ , Fig. 2(d)).

Our method also results in more reliable and reproducible HSAs. Compared to 3D printing, laser cutting is generally limited to specific stock materials and forms. This forces manual adjustment of cutting parameters for each stock material, making fabrication errors more likely to be introduced by the user. These issues are amplified in rotary laser cutting HSAs, especially since

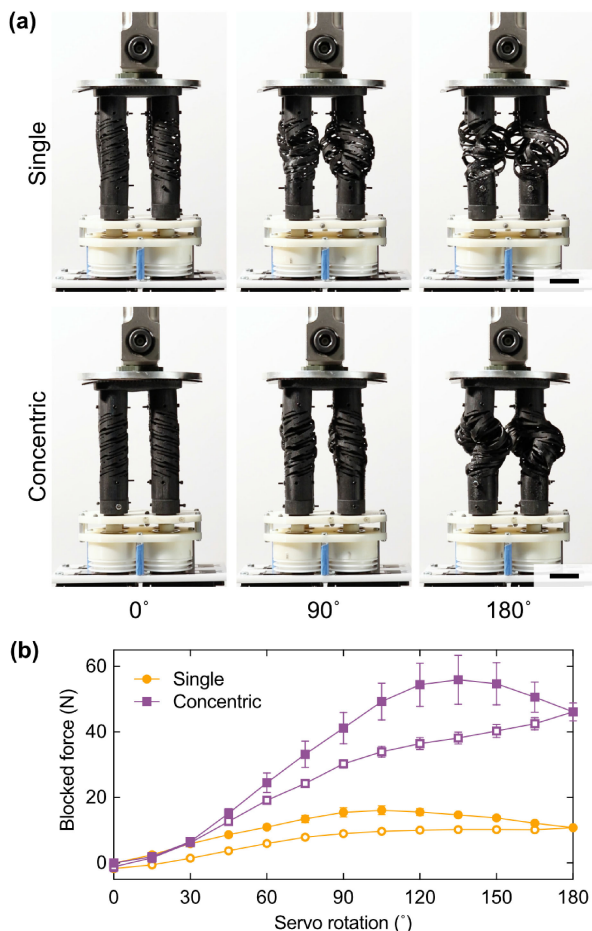


Fig. 5. Blocked force characterization. (a) 4-DoF platforms generate force when elongating. Platforms are shown with four single FPU HSAs (top, all thickness  $T_1$ ) and four concentric FPU HSAs like those in Fig. 2(c) (bottom, all thickness  $T_1$ ) elongating against a load cell. The photographs show the different platforms with servos rotated at  $0^\circ$  (left),  $90^\circ$  (middle), and  $180^\circ$  (right). (b) The corresponding blocked force versus servo rotation angle is provided for the HSA platforms, where filled and open circles correspond to servos rotating from  $0^\circ$  to  $180^\circ$  and  $180^\circ$  to  $0^\circ$ , respectively. Error bars represent standard deviation ( $n = 5$ ). Scale bars are 25 mm.

PTFE tubes are often supplied with variable shape and profile, leading to inconsistent results (Section IIA). By contrast, our 3D printing technique provided more consistent fabrication, especially for the thin, fine constraint features needed for bending in the HSA fingers. This enabled the printing of HSA with  $P_3$  repeat unit scaling, which was never achieved in previous laser-cut HSAs (Fig 2(a)).

### B. Mechanical Characterization

Mechanical characterization data of PTFE, RPU, FPU, and EPU HSAs from tensile and cyclic extension tests are provided in Fig. 3 as the top and bottom row of plots, respectively. As shown in the tensile extension tests in Fig. 3(a) with the original PTFE HSAs, an elongating HSA undergoes three stages of deformation when fixed at one end and allowed to freely rotate at the other. First, the HSA begins to open from its initial closed state, with the living hinges accommodating the auxetic behavior resulting from outward expansion of the individual struts. This opening behavior (from extensions of 0 to  $\sim 80$  mm) requires

little force. Second, as the HSA opens, the struts align along the tensile direction and the structure effectively hardens. The tensile load now primarily acts on the struts, and the force quickly increases, as shown in the J-shaped response up to  $\sim 90$  mm extension. Finally, the struts plastically deform until ultimate failure. Similar deformation responses are reported for other auxetic structures [31]–[34]. From these data and prior works [23], [25], we can interpret that higher forces needed to elongate an HSA correspond to higher torques from a servo motor needed to actuate one.

Most of the RPU, FPU, and EPU HSAs we investigated exhibit similar auxetic behaviors as the original PTFE HSAs. As seen in the tensile extension data in Fig. 3(b), RPU HSAs all elongate under much higher forces than PTFE HSAs given RPU’s higher stiffness, with forces increasing with thickness. RPU HSAs all fail at lower extensions than PTFE HSAs (i.e.,  $\leq 80$  mm extension) due to the living hinges’ inability to accommodate high strains. We observed inconsistent auxetic and mechanical behavior in the thicker  $T_3$  and  $T_4$  RPU HSAs (see Fig. 3(b), (c)) likely due to the restricted living hinge bending in these samples. Of all the printed HSAs, FPU HSAs had the most similar behavior to PTFE HSAs in the extension range of 0 to 100 mm, as seen in Fig. 3(c). As with the PTFE HSAs, the force needed for elongation increases with thickness, although notably, the  $T_3$  and  $T_4$  FPU HSAs could accommodate larger plastic deformations than PTFE HSAs. Finally, as expected from an elastomeric composition, the EPU HSAs extend longer than any other HSAs and elongate under the lowest forces. Mechanical deformation of EPU HSAs is also similar to that in PTFE HSAs from 0 to 100 mm.

As revealed by the cyclic extension data in Fig. 3(a), PTFE HSAs are highly hysteretic given the plastic deformation of the living hinges even under modest HSA extensions. With repeated cycles of tensile extension, the HSAs behave more repeatably. Similar behavior is also observed for the other materials (Fig. 3(b)–(d)). Interestingly, the RPU HSAs failed consistently after only several cycles during experiments at a 10 mm/s elongation rate, and the data shown was obtained with slower extension rates of 1 mm/s (Fig. 3(b)). FPU HSAs appear to have a more pronounced hysteretic behavior than PTFE HSAs (Fig. 3(c)), while that of EPU HSAs is less (Fig. 3(d)), most likely as a result of the EPU HSAs’ living hinges undergoing elastic rather than plastic deformation.

Overall, results from the HSAs’ mechanical characterization suggest that RPU HSAs are not appropriate for use in HSA-based soft robots, given the high servo torques needed to actuate them and their poor robustness to repeated deformations. Conversely, FPU and EPU are promising materials for printed HSAs, and we exclusively used FPU and EPU HSAs for our soft robot demonstrations.

### C. Soft Robot Performance: 4-DoF HSA Platforms

4-DoF HSA platforms are soft robotic systems capable of complex motions for a variety of manipulation and potentially locomotive tasks. As shown in Fig. 4, we assembled HSA platforms from the original platform designs in [23] using PTFE, FPU ( $T_3$ ), and EPU ( $T_5$ ) HSAs (all  $\phi_1$ ). PTFE HSA platforms enable a variety of complex motions, including clockwise (CW) and counter-clockwise (CCW) twisting movements,

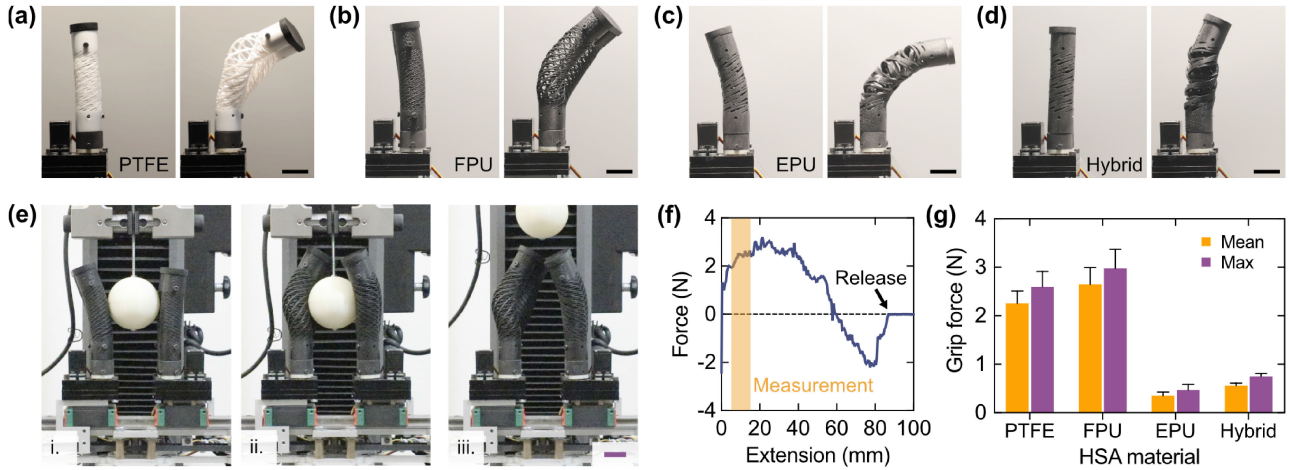


Fig. 6. Soft Robotic Grippers with 3D Printed HSAs. (a-d) Fingers for HSA grippers are designed from bending pairs of HSAs of opposite handedness. (a) PTFE, (b) FPU, (c) EPU, and (d) hybrid rigid-soft bending HSA fingers are shown at rest (left image) and actuated by a programmed servo rotation angle of  $120^\circ$  (right image). (e) Photographs are shown from a video sequence of the FPU gripper during a grip force characterization test. Grip force is measured by positioning HSA grippers around a test object fastened to a load cell (left), bending the fingers (middle), and pulling the test object upwards until it is out of the grippers grasp (right). (F) A plot of force versus extension from the experiment in (e) is provided. The yellow box indicates where the mean average measurement is determined (i.e., between extension of 5 and 15 mm, when the sphere is still contacting the HSA), and the arrow indicates when the object is completely removed from the gripper’s grasp. (G) Grip force analysis for HSA grippers comprised of PTFE, FPU, EPU, and the hybrid HSAs is provided. Error bars represent standard deviation ( $n = 5$ ). Scale bars are 25 mm.

elongations, contractions, and directional bending (Fig. 4(a)). Overall, platforms constructed from FPU HSAs achieve the same types of motions, with qualitatively identical ranges of motion (Fig. 4(b)). Despite their lower hardness and stiffness, EPU platforms also perform similarly (Fig. 4(c)). However, at extreme deformations, we observe the EPU HSAs buckling and limiting the full range of motion.

Previously, concentrically assembled HSAs constructed from spring steel were shown to exhibit interesting load bearing capabilities [25]. With 3D printing enabling the fabrication of custom HSA designs, we are eager to explore how concentrically assembled cylindrical HSAs might open new opportunities for HSA platforms. Future HSA platforms, for example, may require the ability to generate higher forces for various assembly, manufacturing, or locomotive applications. While thicker HSAs could be used to generate higher force, they would also require servos to generate higher or impossible torques. We hypothesize that concentrically assembled thin HSAs would be sufficient to generate a higher blocked force.

Two platforms were constructed from four single FPU HSAs and four concentric FPU HSAs (all  $T_1$ , see Fig. 2(c)). The platforms were actuated to push against a load cell (Fig. 5(a)). The blocked force produced as a function of servo rotation angle in the two platforms is shown in Fig. 5(b). Overall, the max blocked force generated by concentric HSA platforms is approximately 3x greater than that of the single HSA platform. The decrease in blocked force produced by the platforms past a critical servo rotation angle results from the HSAs’ buckling at higher rotation angles. These results demonstrate a new opportunity for improving the performance of HSA-based soft robots by simply nesting custom-sized HSAs together.

#### D. Soft Robot Performance: HSA Grippers

Examples of bending HSA fingers comprised of PTFE ( $T_1$ ) and FPU HSAs ( $T_3$ ) are shown in Figs. 6(a), (b) actuating

after a  $120^\circ$  servo rotation. As expected from their similarity in the 4-DoF platforms, the FPU HSA fingers undergo bending actuation like those laser cut from PTFE. Figs. 6(c), (d) illustrate the performance of the hybrid rigid-soft HSA fingers, without and including the rigid FPU endoskeleton, undergoing similar actuation. The soft EPU HSA fingers ( $T_5$ ) bend to a much greater extent (Fig. 6(c)). The FPU HSA endoskeleton ( $T_3$ ) dramatically reduces overall bending compared to all finger designs but still allows for some bending (Fig. 6(d)).

Representative stills from grip force characterization tests are shown with the FPU HSA gripper in Fig. 6(e). The raw data recorded from the test in Fig. 6(e) is shown in Fig. 6(f), indicating the increase in force on the sphere as it is raised out of the gripper’s hold. At a critical extension, the grip force becomes negative as the tips of the gripper slide around the sphere and press upwards underneath it. Once the sphere is out of the gripper, the force returns to 0 N.

Fig. 6(g) provides the mean and maximum grip forces measured from these characterization experiments. The PTFE HSA gripper provided a mean and maximum grip force of  $2.26 \pm 0.25$  N and  $2.59 \pm 0.32$  N, respectively, while the FPU HSA gripper provided  $2.65 \pm 0.34$  N and  $2.98 \pm 0.39$  N. Within error, the FPU HSA gripper produces similar grip forces to the PTFE one. The softer, less stiff EPU HSA gripper produced a mean and maximum grip force of  $0.35 \pm 0.07$  N and  $0.47 \pm 0.12$  N, respectively. While the current rigid endoskeleton restricts bending motion, it still produces a mean and maximum force of  $0.56 \pm 0.05$  N and  $0.75 \pm 0.06$  N, both of which are greater than the EPU HSA gripper alone. Qualitatively, we observed that the FPU endoskeleton used here required a greater force to elongate than a FPU HSA with  $\phi_1$  and  $T_3$ , suggesting that higher-torque servo motors are needed for this gripper design. With further optimization of the FPU HSA endoskeleton’s design and driving servos, more bioinspired manipulators can potentially be created, where outer EPU HSAs can improve the friction between HSAs and grasped objects and overall

gentleness and adaptability of manipulation, and the inner FPU HSA endoskeletons provide structural stability. The results from the soft platform and gripper experiments confirm that 3D printed HSAs perform similarly to the original PTFE HSAs, and FPU HSAs are qualitatively very similar in behavior to PTFE ones.

#### IV. CONCLUSION

We have shown how an architected material approach to soft robotic actuation can result in a more streamlined, electrically-driven design. By adapting the HSA design for additive manufacturing, we have fabricated HSAs with similar performance as the original designs, while also making a substantial expansion of the HSA design and material space. Not only have we shown two new materials that work in a similar bulk fashion as PTFE, but we have also demonstrated new ways to combine materials that could not have been achieved through traditional off-the-shelf techniques. Whether it's maximizing blocked force through concentric cylinders, enabling new hybrids between rigid and soft materials, or printing a complete finger in a single print (Fig. 1), we have integrated the control of metamaterial design with an electrically-driven actuation strategy via the design flexibility afforded by 3D printing.

While we only explored thickness and diameter variations of original HSA designs in this work, our methods now open opportunities to explore the vast design space of HSAs with digital fabrication techniques and computational design and optimization tools [21], [22]. Once limited to fabricating HSAs via laser cutting of PTFE tubing, we are now exploring what new capabilities – including larger actuation strains, more complex shape changes, and reduced buckling at larger strains – can be introduced through variations of the HSAs' living hinge design, inclusion of features that are truly 3D (i.e., not just the current "2.5-D" forms), and more. While we use digital projection lithography to 3D print our HSAs, other 3D printing methods could be used, provided that they are capable of printing similar materials to FPU and EPU [20], [35]. Overall, we are eager to utilize these methods for the design and fabrication of new electrically-driven soft robots whose architected forms enable progress towards practical systems and applications.

#### REFERENCES

- [1] S. I. Rich, R. J. Wood, and C. Majidi, "Untethered soft robotics," *Nat. Electron.*, vol. 1, no. 2, pp. 102–112, 2018.
- [2] M. Wehner *et al.*, "An integrated design and fabrication strategy for entirely soft, autonomous robots," *Nature*, vol. 536, no. 7617, pp. 451–455, 2016.
- [3] E. Acome *et al.*, "Hydraulically amplified self-healing electrostatic actuators with muscle-like performance," *Science*, vol. 359, no. 6371, pp. 61–65, 2018.
- [4] M. Duduta, E. Hajiesmaili, H. Zhao, R. J. Wood, and D. R. Clarke, "Realizing the potential of dielectric elastomer artificial muscles," *Proc. Nat. Academy Sci.*, vol. 116, no. 7, pp. 2476–2481, 2019.
- [5] A. Miriyev, K. Stack, and H. Lipson, "Soft material for soft actuators," *Nat. Commun.*, vol. 8, no. 1, 2017, Art. no. 596.
- [6] Q. He, Z. Wang, Y. Wang, A. Minori, M. T. Tolley, and S. Cai, "Electrically controlled liquid crystal elastomer-based soft tubular actuator with multimodal actuation," *Sci. Adv.*, vol. 5, no. 10, 2019, Art. no. eaax5746.
- [7] M. J. Ford *et al.*, "A multifunctional shape-morphing elastomer with liquid metal inclusions," *Proc. Nat. Academy Sci.*, vol. 116, no. 43, pp. 21438–21444, 2019.
- [8] A. Rafsanjani, K. Bertoldi, and A. R. Studart, "Programming soft robots with flexible mechanical metamaterials," *Sci. Robot.*, vol. 4, no. 29, 2019, Art. no. eaav7874.
- [9] K. Bertoldi, V. Vitelli, J. Christensen, and M. van Hecke, "Flexible mechanical metamaterials," *Nat. Rev. Mater.*, vol. 2, no. 11, 2017, Art. no. 17066.
- [10] M. Kaur and W. S. Kim, "Toward a smart compliant robotic gripper equipped with 3D-designed cellular fingers," *Adv. Intell. Syst.*, vol. 1, no. 3, 2019, Art. no. 1900019.
- [11] B. Gorissen, D. Melancon, N. Vasios, M. Torbati, and K. Bertoldi, "Inflatable soft jumper inspired by shell snapping," *Sci. Robot.*, vol. 5, no. 42, pp. 1–7, 2020, Art. no. eabb1967.
- [12] J. Overvelde *et al.*, "A three-dimensional actuated origami-inspired transformable metamaterial with multiple degrees of freedom," *Nat. Commun.*, vol. 7, 2016, Art. no. 10929.
- [13] P. Rothemund *et al.*, "A soft, bistable valve for autonomous control of soft actuators," *Sci. Robot.*, vol. 3, no. 16, 2018, Art. no. eaar7986.
- [14] Y. Jiang, L. M. Korpas, and J. R. Raney, "Bifurcation-based embodied logic and autonomous actuation," *Nat. Commun.*, vol. 10, no. 1, 2019, Art. no. 128.
- [15] T. Chen, O. R. Bilal, K. Shea, and C. Daraio, "Harnessing bistability for directional propulsion of soft, untethered robots," *Proc. Nat. Academy Sci.*, vol. 115, no. 22, pp. 5698–5702, 2018.
- [16] T. G. Thuruthel, S. Haider Abidi, M. Cianchetti, C. Laschi, and E. Falotico, "A bistable soft gripper with mechanically embedded sensing and actuation for fast grasping," in *Proc. IEEE Int. Conf. Robot Hum. Interactive Commun.*, 2020, pp. 1049–1054.
- [17] A. Rafsanjani, Y. Zhang, B. Liu, S. M. Rubinstein, and K. Bertoldi, "Kirigami skins make a simple soft actuator crawl," *Sci. Robot.*, vol. 3, no. 15, 2018, Art. no. eaar7555.
- [18] A. Lazarus and P. M. Reis, "Soft actuation of structured cylinders through auxetic behavior," *Adv. Eng. Mater.*, vol. 17, no. 6, pp. 815–820, 2015.
- [19] D. Yang *et al.*, "Buckling pneumatic linear actuators inspired by muscle," *Adv. Mater. Technol.*, vol. 1, no. 3, 2016, Art. no. 1600055.
- [20] R. L. Truby and J. A. Lewis, "Printing soft matter in three dimensions," *Nature*, vol. 540, no. 7633, pp. 371–378, Dec. 2016.
- [21] A. Clausen, F. Wang, J. S. Jensen, O. Sigmund, and J. A. Lewis, "Topology optimized architectures with programmable poisson's ratio over large deformations," *Adv. Mater.*, vol. 27, no. 37, pp. 5523–5527, 2015.
- [22] M. Konaković, K. Crane, B. Deng, S. Bouaziz, D. Piker, and M. Pauly, "Beyond developable: Computational design and fabrication with auxetic materials," *ACM Trans. Graph.*, vol. 35, no. 4, pp. 1–11, Jul. 2016.
- [23] L. Chin, J. Lipton, R. MacCurdy, J. Romanishin, C. Sharma, and D. Rus, "Compliant electric actuators based on handed shearing auxetics," in *Proc. IEEE Int. Conf. Soft Robot.*, 2018, pp. 100–107.
- [24] L. Chin, J. Lipton, M. C. Yuen, R. Kramer-Bottiglio, and D. Rus, "Automated recycling separation enabled by soft robotic material classification," in *Proc. IEEE Int. Conf. Soft Robot.*, 2019, pp. 102–107.
- [25] J. I. Lipton, R. MacCurdy, Z. Manchester, L. Chin, D. Cellucci, and D. Rus, "Handedness in shearing auxetics creates rigid and compliant structures," *Science*, vol. 360, no. 6389, pp. 632–635, 2018.
- [26] Zeus Industrial Products, PTFE Polymer Technical Sheet, 2020. [Online]. Available: <https://www.zeusinc.com/materials/ptfe/>
- [27] Carbon, Inc., *RPU 70 Technical Datasheet*, Carbon, Inc., Redwood City, CA, 2020. [Online]. Available: <https://www.carbon3d.com/materials/rpu-70/>
- [28] Carbon, Inc., *FPU 50 Technical Datasheet*, Carbon, Inc., Redwood City, CA, 2020. [Online]. Available: <https://www.carbon3d.com/materials/fpu-50/>
- [29] Carbon, Inc., *EPU 40 Technical Datasheet*, Carbon, Inc., Redwood City, CA, 2020. [Online]. Available: <https://www.carbon3d.com/materials/epu-40/>
- [30] L. Chin, F. Barscevicus, J. Lipton, and D. Rus, "Multiplexed manipulation: Versatile multimodal grasping via a hybrid soft gripper," in *Proc. IEEE Int. Conf. Robot. Autom.*, 2020, pp. 8949–8955.
- [31] J. Zhang, G. Lu, Z. Wang, D. Ruan, A. Alomarah, and Y. Durandet, "Large deformation of an auxetic structure in tension: Experiments and finite element analysis," *Compos. Struct.*, vol. 184, pp. 92–101, 2018.
- [32] Y. Jiang and Y. Li, "3D printed auxetic mechanical metamaterial with chiral cells and re-entrant cores," *Sci. Rep.*, vol. 8, no. 1, 2018, Art. no. 2397.
- [33] P. Celli *et al.*, "Shape-morphing architected sheets with non-periodic cut patterns," *Soft Matter*, vol. 14, pp. 9744–9749, 2018.
- [34] X. Xin, L. Liu, Y. Liu, and J. Leng, "4D printing auxetic metamaterials with tunable, programmable, and reconfigurable mechanical properties," *Adv. Funct. Mater.*, vol. 30, 2020, Art. no. 2004226.
- [35] D. Chen and X. Zheng, "Multi-material additive manufacturing of metamaterials with giant, tailorable negative poisson's ratios," *Sci. Rep.*, vol. 8, no. 1, 2018, Art. no. 9139.